TU Delft

Delft University of Technology

Prediction of oedometer terminal densities through a memory-enhanced cyclic model for sand

Liu, Haoyuan; Pisano, Federico

DOI
10.1680/jgele.18.00187

Publication date
2019

Document Version
Accepted author manuscript

Published in
Geotechnique Letters (Online)

Citation (APA)
Liu, H., & Pisano, F. (2019). Prediction of oedometer terminal densities through a memory-enhanced cyclic model for sand. *Geotechnique Letters (Online)*, *9*(2), 81-88. https://doi.org/10.1680/jgele.18.00187

Important note
To cite this publication, please use the final published version (if applicable).
Please check the document version above.

Copyright
Other than for strictly personal use, it is not permitted to download, forward or distribute the text or part of it, without the consent of the author(s) and/or copyright holder(s), unless the work is under an open content license such as Creative Commons.

Takedown policy
Please contact us and provide details if you believe this document breaches copyrights.
We will remove access to the work immediately and investigate your claim.

This work is downloaded from Delft University of Technology.
For technical reasons the number of authors shown on this cover page is limited to a maximum of 10.

Géotechnique Letters **00**, 1–7, http://dx.doi.org/10.1680/geolett.XX.XXXXX

Prediction of oedometer terminal densities through a memory-enhanced plasticity model for sand

H. Y. LIU*, F. PISANÒ*

Predicting the cyclic response of soils is still challenging in many geotechnical fields, and motivates massive research to shed light on lesser-known aspects of the problem. In this area, the continual efforts on the constitutive modelling of cyclic sand behaviour demand new and reliable dataset for model validation – especially for loading conditions involving many loading cycles ('high-cyclic' loading). In this letter, the recent memory-enhanced bounding surface formulation by Liu *et al.* (2018a) is considered as a suitable platform to reproduce the high-cyclic response of sands, and its transition into either 'ratcheting' or 'shakedown' behaviour. New evidence of its suitability is found against the latest dataset presented in Park & Santamarina (2018), comprising the results of high-cyclic oedometer tests at varying initial/loading conditions. Model-simulations prove in satisfactory agreement with most experimental findings, especially regarding the prediction of so-called 'terminal densities'.

KEYWORDS: sands; stiffness; settlement; constitutive relations; plasticity; numerical modelling

ICE Publishing: all rights reserved

INTRODUCTION

Cyclically-loaded foundations may suffer from permanent displacements/rotations depending on the cyclic soil response turning into either 'ratcheting' (gradual/steady plastic strain accumulation) or 'shakedown' (no net strain accumulation over a full cycle) (Houlsby *et al.*, 2017). Presently, this issue is attracting special attention in relation to monopiles for offshore wind turbines, that must be designed to ensure proper operational performance under up to 10^8-10^9 loading cycles (LeBlanc *et al.*, 2010; DNV, 2016; Byrne *et al.*, 2017) – 'high-cyclic' loading.

Cyclic strain accumulation in soils is often described through empirical formulas based on laboratory test results (Lekarp & Dawson, 1998; Wichtmann, 2005), with clear limitations set by the costs/timing of high-cyclic testing. Alternatively, strain accumulation may also be predicted via advanced constitutive models, that can contribute to the cyclic analysis of foundations in at least two ways:

(i) in so-called 'explicit' methods, by providing model-based strain accumulation relationships for calculations driven by increasing number of cycles – rather than physical time-stepping (Pasten *et al.*, 2013; Jostad *et al.*, 2014; Triantafyllidis *et al.*, 2016);
(ii) in traditional 'implicit' approaches, by reproducing the cyclic stress-strain response in step-by-step, time-domain simulations of 'affordable' duration (Corciulo *et al.*, 2017; Kementzetzidis *et al.*, 2018a,b).

In either case the need for robust cyclic models validated against wide experimental evidence is self-apparent. At the same time, the dearth of high-cyclic dataset should also be recognised as a serious hurdle against the final goal.

This letter takes a step forward about the application of soil plasticity models to high-cyclic geotechnical problems, particularly of the new memory-enhanced bounding surface formulation for sand by Liu *et al.* (Liu *et al.*, 2018a,b). The model belongs in the well-known family of critical-state SANISAND models (Dafalias & Manzari, 2004), and relies on the use of an additional locus ('memory surface') to capture fabric-related ratcheting/shakedown phenomena (Corti *et al.*, 2016). An opportunity for building further trust about the model has been very recently offered by Park & Santamarina (2018), who published novel data concerning dry sand compaction in high-cyclic oedometer tests (i.e. under 'zero-lateral-strain' loading). Although seldom considered in experiments (Wichtmann, 2005; Wichtmann & Triantafyllidis, 2016), high-cyclic oedometer compaction is most relevant to the performance of offshore foundations and not only – for instance regarding the analysis of 'push-pull' mechanisms under multi-legged structures (Bienen *et al.*, 2018; Pisanò *et al.*, 2019), or vibratory pile driving (Galavi *et al.*, 2017).

This work aims to bring new evidence about the capabilities of Liu *et al.*'s model, with emphasis on the prediction of 'terminal densities' (Narsilio & Santamarina, 2008) and associated stiffness evolution.

REFERENCE HIGH-CYCLIC OEDOMETER TESTS

Following Chong & Santamarina (2016), Park & Santamarina (2018) performed an extensive experimental programme to investigate the response of dry sand in high-cyclic oedometer tests. Vertical stress-strain loops and variations in void ratio were obtained for each test, along with bender element measurements of the shear wave velocity. Park & Santamarina's work revolves around the concept of 'terminal density', referring to cyclically loaded sands eventually approaching an asymptotic (terminal) void ratio (density). In reflection of initial fabric, sands evolve towards terminal densities depending mechanical properties, loading programme and boundary conditions (Dappolonia & Dappolonia, 1967; Lackenby *et al.*, 2007; Narsilio & Santamarina, 2008).

The following features of Park & Santamarina's tests are relevant to remainder of this work:

Manuscript received. . .
Published online at www.geotechniqueletters.com
* Faculty of Civil Engineering and Geosciences, Delft University of Technology, Stevinweg 1, 2628 CN Delft (The Netherlands)

Table 1. Test conditions in Park & Santamarina (2018) – D_{r0}: initial relative density, e_0: initial void ratio, σ_0: pre-cyclic vertical stress, $\Delta\sigma$: cyclic stress amplitude, $\Delta\sigma/\sigma_0$: cyclic stress amplitude ratio.

Test #	D_{r0} [%]	e_0 [–]	σ_0 [kPa]	$\Delta\sigma$ [kPa]	$\Delta\sigma/\sigma_0$ [–]
1	30	0.6700	67	100	1.5
2	40	0.6460	174	138	0.8
3	40	0.6460	105	138	1.3
4	40	0.6460	105	276	2.7
5	40	0.6460	105	414	4
6	50	0.6220	67	100	1.5
7	70	0.5740	174	138	0.8
8	70	0.5740	105	138	1.3
9	70	0.5740	67	100	1.5
10	70	0.5740	105	276	2.7
11	70	0.5740	105	414	4

- tests performed on Ottawa 20/30 sand with $D_{50} = 0.72$ mm, $e_{max} = 0.742$, $e_{min} = 0.502$, $G_s = 2.65$;
- four-stage loading sequence: (i) static compression up to σ_0, (ii) cyclic loading of amplitude $\Delta\sigma$ between σ_0 and $\sigma_0 + \Delta\sigma$, (iii) static compression to the maximum vertical stress $\sigma_{max} > \sigma_0 + \Delta\sigma$, (iv) unloading;
- 33 tests in total (including repetitions), with 11 different combinations of initial/loading conditions and number of cycles $N = 10^4$.

Relevant test settings considered are all summarised in Table 1*.

A SANISAND MODEL WITH RATCHETING CONTROL

This section recalls the main features of the sand model by Liu *et al.* (2018a), whilst formulation and link to literature are detailed in the original publication. The calibration of model parameters for Ottawa 20/30 sand is also covered.

Formulation and governing parameters

Liu *et al.*'s model is built upon the parent SANISAND04 model by Dafalias & Manzari (2004), and enhanced according to the notion of memory surface (Corti *et al.*, 2016). The memory locus is introduced to track fabric effects, and hence simulate realistic sand behaviour under high-cyclic loading. Compared to SANISAND04, Liu *et al.* (2018a) introduced in the normalised π-plane a third circular locus, the memory surface (Figure 1a), which evolves during soil straining so as to (i) modify its size/position in reflection of fabric changes, (ii) always enclose the yield surface, (iii) influence changes in sand stiffness and dilatancy. Most other ingredients of SANISAND04 were instead kept unaltered.

The memory surface governs the evolution of sand stiffness through the plastic modulus K_p (Dafalias & Manzari, 2004):

$$K_p = \frac{2}{3} p h (\mathbf{r}^b - \mathbf{r}) : \mathbf{n} \tag{1}$$

K_p depends not only on the distance between current stress ratio ($\mathbf{r}$) and its image point on the bounding surface ($\mathbf{r}^b$), but also on the distance between $\mathbf{r}$ and its projection on the memory surface $\mathbf{r}^M$ (along the normal to the yield surface at current $\mathbf{r}$). The latter feature stems from a re-definition of the hardening coefficient h in Equation (1):

$$h = \frac{b_0}{(\mathbf{r} - \mathbf{r}_{in}) : \mathbf{n}} \exp\left[\mu_0 \left(\frac{p}{p_{atm}}\right)^{0.5} \left(\frac{b^M}{b_{ref}}\right)^2\right] \tag{2}$$

The memory-related parameter μ_0 links fabric effects to soil stiffness, with major influence on drained cyclic strain accumulation, or equivalently on the rate of pore pressure build-up under undrained conditions (Liu *et al.*, 2018b). Relevant to predictive capability is also the presence of the pressure-dependent term $(p/p_{atm})^{0.5}$ term in Equation (2) (Corti *et al.*, 2017; Liu *et al.*, 2018a).

Evolution laws for the memory surface, namely for the memory back-stress $\boldsymbol{\alpha}^M$ and size m^M, were inspired by experimental evidence (Liu *et al.*, 2018a). As contractive soil behaviour promotes 'fabric reinforcement', stages of cyclic contraction were linked to an expansion of the memory surface ($dm^M > 0$), and therefore to gradual stiffening through Equations (1)–(2). In contrast, dilative deformation is known to weaken the granular microstructure ('fabric damage'), so that a shrinkage of the memory surface ($dm^M < 0$) was introduced to capture stiffness losses due to (unconstrained) dilation. Overall, the evolution of m^M is determined by Equation (3):

$$dm^M = \sqrt{\frac{3}{2}} d\boldsymbol{\alpha}^M : \boldsymbol{n} - \frac{m^M}{\zeta} f_{shr} \left\langle -d\varepsilon_v^p \right\rangle \tag{3}$$

in which the last term on the right-hand side rules the mentioned shrinking mechanism through the model parameter ζ.

Finally, the memory locus was also exploited to capture the higher contractancy exhibited by the sand when unloaded after dilative deformation – a phenomenon usually associated to 'fabric re-orientation' and modelled in SANISAND04 through the concept of 'fabric tensor'. Liu *et al.* (2018a) proposed the following re-definition of SANISAND04's dilatancy coefficient (D):

$$D = A_d(\boldsymbol{r}^d - \boldsymbol{r}) : \boldsymbol{n}, \qquad A_d = A_0 \exp\left(\beta \frac{\left\langle \tilde{b}_d^M \right\rangle}{b_{ref}}\right) \tag{4}$$

With the visual support of Figure 1c, Equation (4) sets the distance $\tilde{b}_d^M = (\tilde{\mathbf{r}}^d - \tilde{\mathbf{r}}^M) : \mathbf{n}$ to establish whether the sand is more or less prone to volume changes by modulating the magnitude of D. The enhancement of post-dilation contractancy depends on the material parameter β in Equation (4), only effective when the soil has dilated before load increment reversal.

The SANISAND04 model enhanced with the above ingredients has already proven suitable to reproduce cyclic ratcheting in drained laboratory tests (Liu *et al.*, 2018b). The case of cyclic oedometer compaction was preliminarily considered in relation to the test results by Chong & Santamarina (2016), though with no attempt to capture the monotonic compression preceding cyclic loading. Since SANISAND models with an uncapped yield locus cannot predict such a monotonic response (Taiebat & Dafalias, 2008), only cyclic quotas of oedometer compaction will be examined in the following.

Parameter calibration for Ottawa 20/30 sand

Liu *et al.*'s model requires overall the calibration of sixteen parameters: thirteen inherited from SANISAND04, three newly introduced in Equations (2)–(4). All model parameters have

*In Park & Santamarina (2018) and in this work, e_0 denotes the initial void ratio at the start of cyclic loading ('pre-cyclic' void ratio).

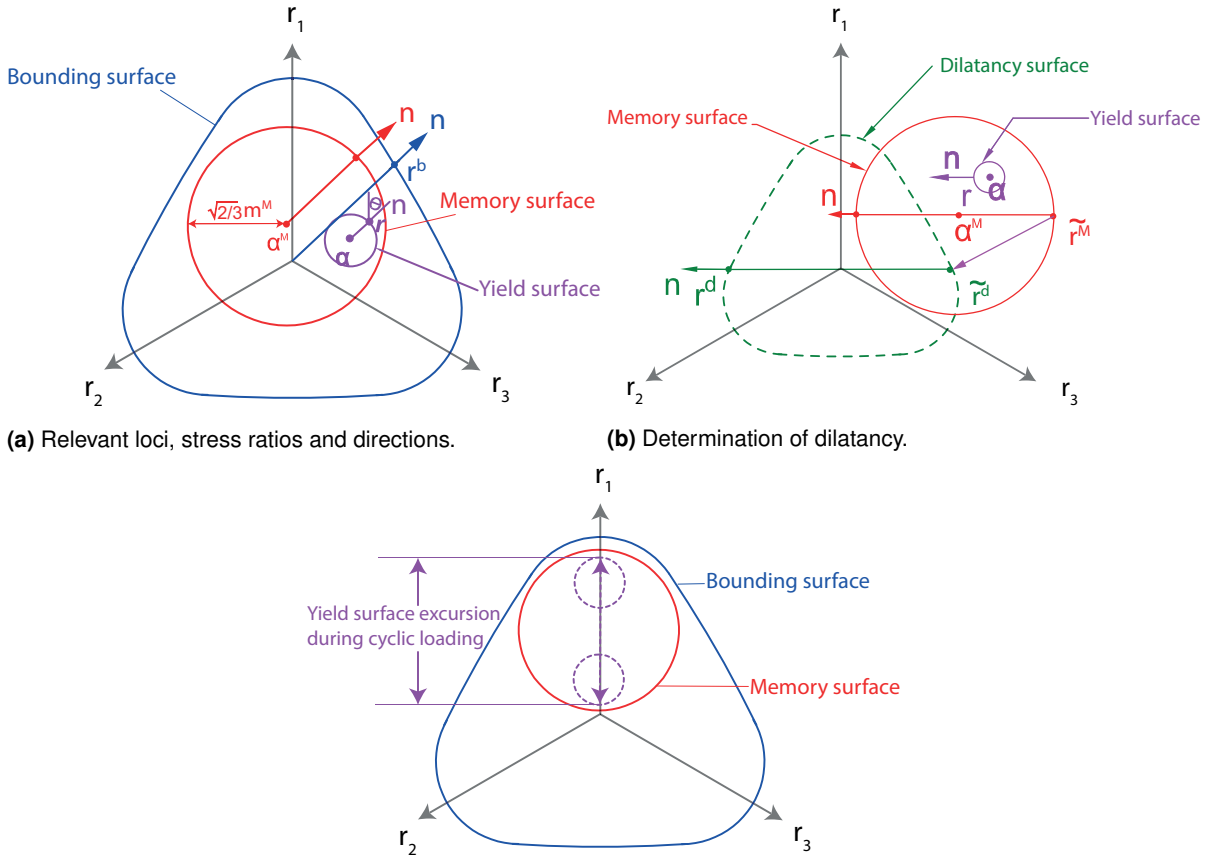

(a) Relevant loci, stress ratios and directions.

(b) Determination of dilatancy.

(c) Stress path of oedometer tests.

Fig. 1. The memory-enhanced sand model by Liu *et al.* (2018a).

Table 2. Model parameters for the Ottawa 20/30 sand tested by Park & Santamarina (2018)

Elasticity		Critical state					Yield surface	Plastic modulus			Dilatancy		Memory surface		
G_0	ν	M_c	c	λ_c	e_0	ξ	m	h_0	c_h	n^b	A_0	n^d	μ_0	ζ	β
160	0.05	1.12	0.75	0.025	0.732	0.6	0.01	4.8	1.2	2.68	0.71	1.20	200	0.005	0.5

been identified following the procedure in Liu *et al.* (2018a), and never modified for prediction purposes. Table 2 reports the parameter set for Ottawa 20/30 sand, calibrated against literature data from different sources. The test results from Santamarina & Cho (2001) ('simple critical state tests') and Lin *et al.* (2015) (drained monotonic triaxial tests) allowed to determine the first thirteen parameters (from G_0 to n^d in the table). Only two tests out of Park & Santamarina's dataset were employed to calibrate memory-related parameters – μ_0, ζ and β – in two steps:

1. high-cyclic loading ($N = 10^4$, $\sigma_0 = 105$ kPa, $\Delta\sigma = 138$ kPa) on a loose sample ($e_0 = 0.631$) was first considered to identify μ_0 far from dilatancy effects (i.e. with no influence of ζ and β). Setting $\mu_0 = 200$ allowed to simulate the same cyclic reduction in void ratio e measured experimentally – compare Figures 2a-2c;
2. keeping the same $\mu_0 = 200$ value, the (ζ, β) pair was calibrated by matching the high-cyclic response of a denser sample ($e_0 = 0.5342$) subjected to the same loading programme – compare Figures 2d-2f.

Since the model is inherently unsuitable for monotonic oedometer loading, an iterative procedure was established to transit from an assumed initial void ratio e_{in} to the target pre-cyclic value e_0. This procedure enabled the pre-cyclic initialisation of all hardening variables, and to finally obtain μ_0-ζ-β values in good agreement with those calibrated in Liu *et al.* (2018a) for the quartz sand tested by Wichtmann (2005).

Empirical compaction trends

The same results in Figure 2 can be re-compared based on the following empirical relationship by Park & Santamarina (2018):

$$e_i = e_T + (e_1 - e_T)\left[1 + \left(\frac{i-1}{N^*}\right)^m\right]^{-1} \tag{5}$$

For oedometer high-cyclic conditions, Equation (5) estimates the void ratio e_i at the i^{th} loading cycle as a function of:

(i) the terminal void ratio e_T ($e_i \to e_T$ as $i \to \infty$);
(ii) the characteristic number of cycles N^*, informing about the number of cycles $1 + N^*$ needed for half of the total compaction $(e_1 - e_T)/2$ to occur;
(iii) an empirical exponent m found in the order of $m = 0.45 \pm 0.05$ for oedometer conditions (Park & Santamarina, 2018).

Park & Santamarina (2018) fitted experimental compaction trends by identifying N^* in Equation (5), so as to predict e_T when taking more than 10^4 cycles to be attained. For comparison, the same has been done here for the simulated

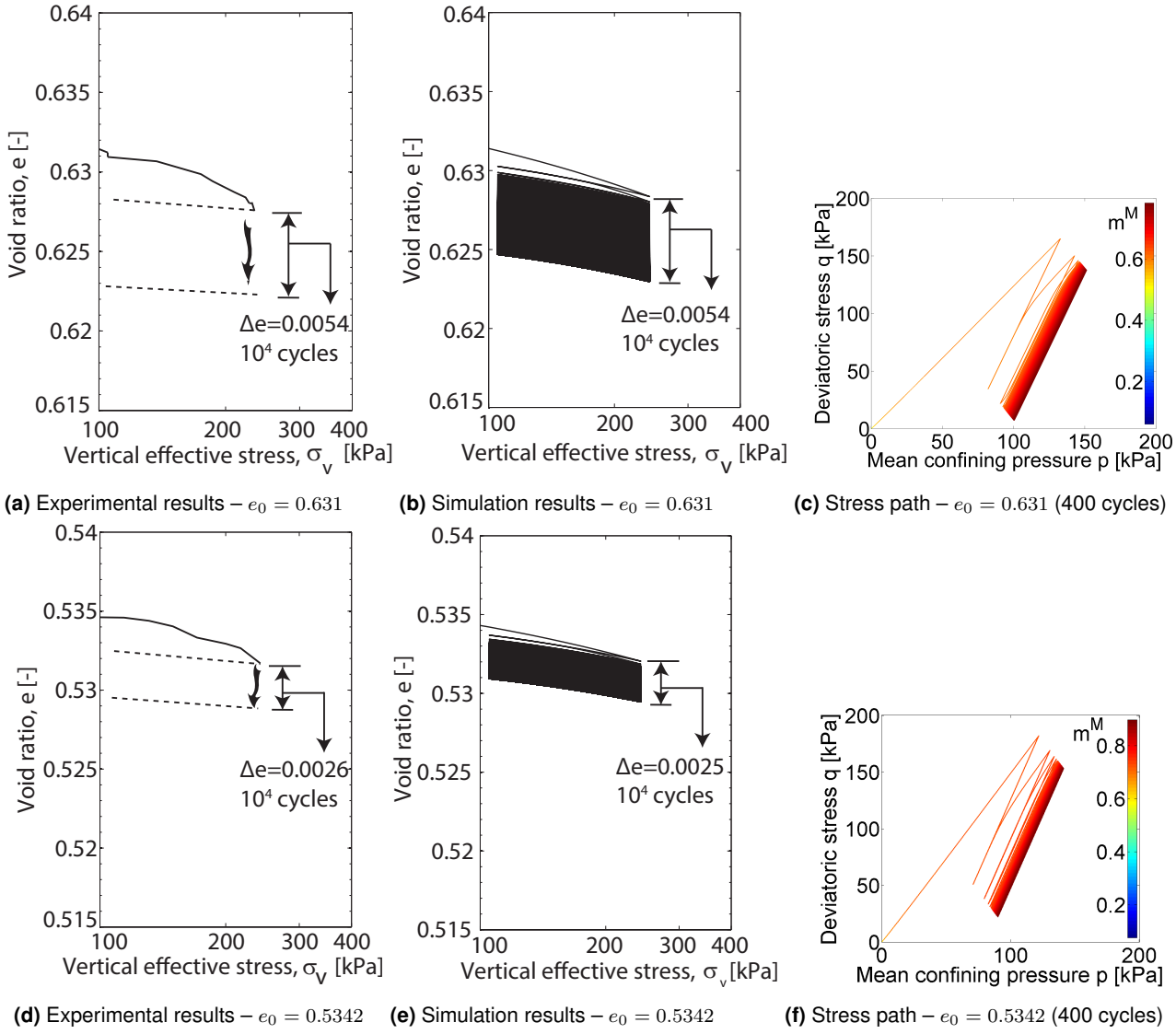

(a) Experimental results – $e_0 = 0.631$ **(b)** Simulation results – $e_0 = 0.631$ **(c)** Stress path – $e_0 = 0.631$ (400 cycles)

(d) Experimental results – $e_0 = 0.5342$ **(e)** Simulation results – $e_0 = 0.5342$ **(f)** Stress path – $e_0 = 0.5342$ (400 cycles)

Fig. 2. Comparison between Park & Santamarina's experimental results and memory-surface-based simulations in terms of cyclic compaction for a loose and a dense sand sample. Oedometer est conditions: $\sigma_0 = 105$ kPa, $\Delta\sigma = 138$ kPa, $N = 10^4$.

Table 3. Estimated terminal density e_T and character number of cycles N^* based on Park & Santamarina's experimental results and memory-surface-based simulation presented in Figure 2.

	bound	D_{r0}	m	N^*	e_T
Exp	upper	44%	0.4	350	0.6213
		86%		200	0.5288
	lower	44%		200	0.6209
		86%		200	0.5284
Sim	upper	44%	0.45	794	0.6227
		86%		631	0.5303
	lower	44%		1291	0.6208
		86%		1111	0.5287

compaction trends, as shown in Figure 3 with respect to $e - N$ curves associated with the same tests in Figure 2. Specifically, numerical cyclic responses (grey lines) are plotted along with the associated upper/lower bounding curves obtained through Equation (5) (red lines), as well as with the curves identified by Park & Santamarina (2018) as experimental bounds (black lines).

Although somewhat different in terms of identified (N^*, m) pairs, experiment-based and simulation-based bounding curves provide consistent estimates of the terminal void ratio e_T – see Figure 3 and Table 3. Therefore, Liu *et al.*'s model can be used to reliably predict high-cyclic compaction, and extrapolate credible e_T values through Equation (5) for $N \to \infty$.

MODEL PREDICTION OF TERMINAL DENSITIES

The model performance as resulting from the parameter set in Table 2 is now evaluated against Park & Santamarina's test results. Model simulations were performed for the the eleven testing scenarios in Table 1, including different relative densities ($30\% < D_r < 70\%$) and cyclic stress amplitude ratios ($0.8 < \Delta\sigma/\sigma_0 < 4$). In all cases, the lower bounds of numerical $e - N$ compaction curves were identified by setting $m = 0.45$ in Equation (5) and looking for suitable N^* values. The obtained bounding curves were then used to infer e_T for $N \to \infty$ and compare to experimental results.

In Figure 4 experimental and numerical findings are compared in terms of relation between terminal (e_T) and initial void (e_0) ratios at varying cyclic stress amplitude ratios $\Delta\sigma/\sigma_0$.

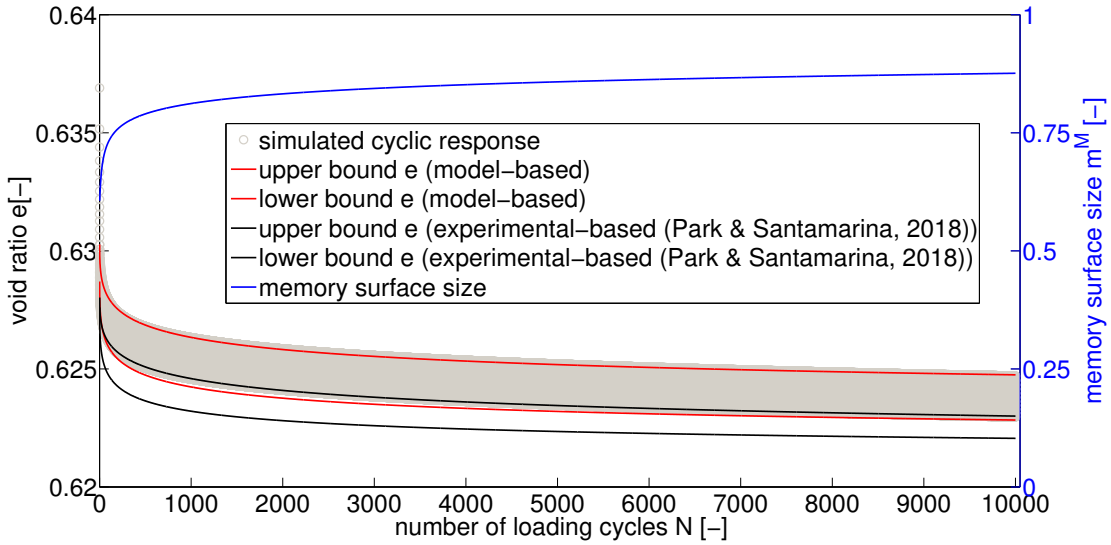

(a) Pre-cyclic void ratio $e_0 = 0.631$

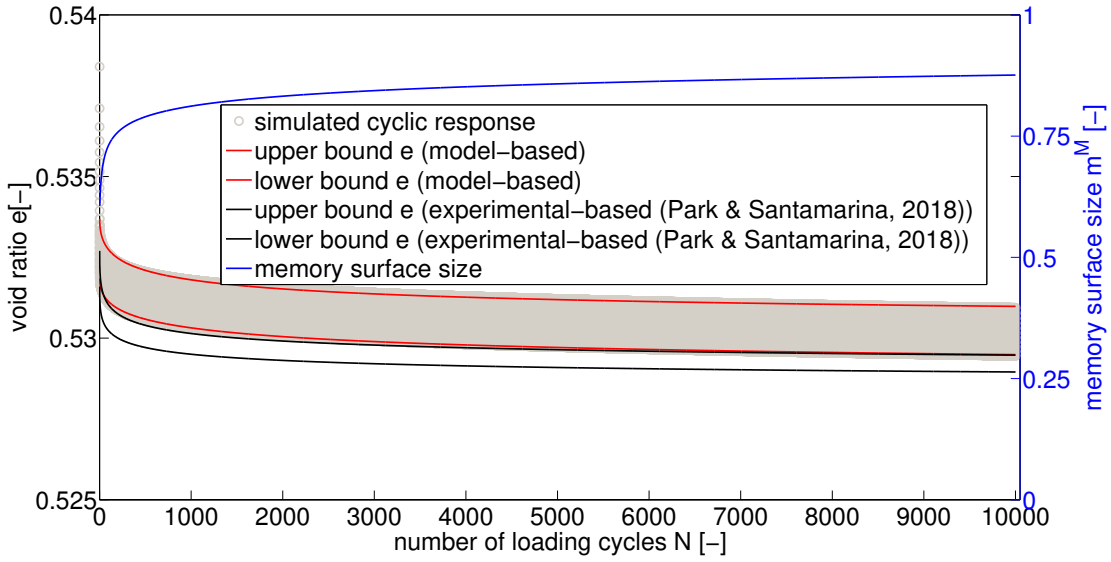

(b) Pre-cyclic void ratio $e_0 = 0.5342$

Fig. 3. Void ratio evolution over $N = 10^4$ loading cycles for loose and dense sand samples (Park & Santamarina, 2018) – pre-cyclic vertical stress $\sigma_0 = 105$ kPa, cyclic stress amplitude $\Delta\sigma = 138$ kPa.

Beyond being in good agreement with experimental data, the results of model simulations confirm that: (i) at given e_0, e_T tends to decrease for higher $\Delta\sigma/\sigma_0$; (ii) lowest initial e_0 values lead to lowest e_T at given $\Delta\sigma/\sigma_0$. Although sands evolve towards different fabric configurations depending on properties and loading, the memory of the initial state will not be erased (López-Querol & Coop, 2012; Chong & Santamarina, 2016; Park & Santamarina, 2018). Park & Santamarina (2018) also post-processed their experimental results in terms of dimensionless volume contraction λ:

$$\lambda = \frac{e_T - e_{min}}{e_0 - e_{min}} \tag{6}$$

which was found to depend linearly on $\Delta\sigma/\sigma_0$. The same empirical trend emerges fairly well also from the model predictions in Figure 5 over the whole $\Delta\sigma/\sigma_0$ range considered ($0.8 < \Delta\sigma/\sigma_0 < 4$).

Additionally, Park & Santamarina (2018) inspected experimental compaction trends also in terms of maximum/terminal variations in relative density (ΔD_T):

$$\Delta D_T = \frac{e_0 - e_T}{e_{max} - e_{min}} \tag{7}$$

and recognised a dependence on the cyclic stress amplitude ratio of the following kind ($D_{i=0}$ represents in Equation (8) the pre-cyclic relative density):

$$\Delta D_T = \frac{(\Delta\sigma/\sigma_0)(1 - D_{i=0})^n}{B} \tag{8}$$

with estimated parameters $B \approx 20 \div 25$ and $n = 0.7$ for Ottawa 20/30 sand. Model-based predictions of ΔD_T for all eleven scenarios (Table 1) are compared to experiment-based trend lines in Figure 6, where different marker shapes/colours correspond to different $\Delta\sigma/\sigma_0$ values. The memory-enhanced model appears to predict with reasonable accuracy the non-linear $\Delta D_T - D_{i=0}$ relationship for all cyclic stress ratios.

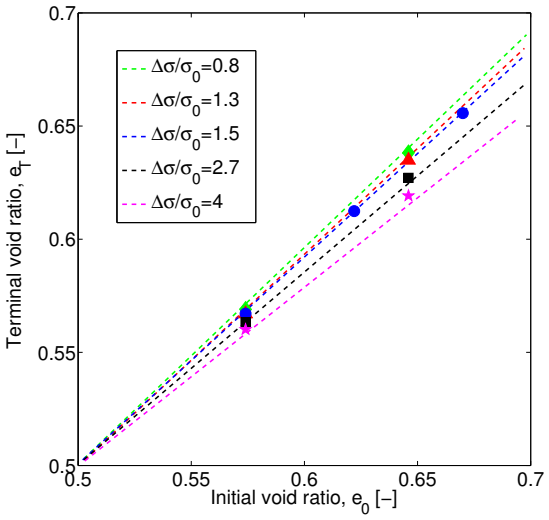

Fig. 4. Relation between terminal and initial void ratios for different cyclic stress ratios – dash lines: interpolation of Park & Santamarina's data; markers: model simulations; same colours assigned to related dash lines and markers.

Evolution of constrained modulus

Park & Santamarina (2018) found experimentally a practical correlation between the shear wave velocity V_s (obtained from bender element measurements) and the following constrained modulus M^{oed} relevant to 1D compression problems:

$$M_i^{oed} = \frac{\Delta\sigma}{\Delta\varepsilon_i^{pp}} \tag{9}$$

In equation (9) $\Delta\varepsilon_{pp}^{i}$ denotes the peak-to-peak amplitude of the i^{th} vertical strain loop – derived as usual from variations in void ratio, $\Delta\varepsilon_i^{pp} = -\Delta e_i/(1+e_i)$.

As the secant/cyclic M^{oed} evolves over cycles, model simulation results can be similarly post-processed to obtain numerical predictions of the varying sand stiffness. Figure 7 presents a comparison between experimental and numerical results in terms of constrained modulus normalised with respect to its first cycle value, i.e. $M_i = M_i^{oed}/M_1^{oed}$ – plots relate to both dense and loose samples subjected to cyclic stress amplitude ratios $\Delta\sigma/\sigma_0$ equal to 1.3 (Figure 7a), 2.7 (Figure 7b) and 4 (Figure 7c).

Experimental and numerical stiffness trends prove in very good agreement over the whole range of loading cycles, and confirm the expected increase in M^{oed} due to high-cyclic densification.

CONCLUDING REMARKS

The results from newly published experimental and modelling works were compared with respect to the high-cyclic response of sands under 1D oedometer compression. The adopted constitutive modelling, based on memory-enhanced bounding surface plasticity, proved capable of predicting cyclic oedometer compaction over a wide range of loading cycles, void ratios and cyclic stress amplitude ratios. In particular, terminal void ratios (densities) were well captured in all cases, with correct dependencies on relevant factors considered in the parametric studies.

This study added evidence regarding the suitability of the memory/bounding surface framework for high-cyclic geotechnical problems. Building trust about these modelling tools helps the transition towards constitutive models used in support (or, eventually, replacement) of expensive experimental programmes when empirical cyclic strain accumulation laws are demanded – e.g. in offshore, railway and earthquake geotechnics.

ACKNOWLEDGEMENTS

The authors wish to acknowledge the China Scholarship Council (CSC) and the Geo-Engineering Section of Delft University of Technology for financial support of the first author.

REFERENCES

Bienen, B., Klinkvort, R. T., O'Loughlin, C., Zhu, F. & Byrne, B. (2018). Suction caissons in dense sand, part ii: vertical cyclic loading into tension. *Géotechnique* , 1–15.

Byrne, B., McAdam, R., Burd, H., Houlsby, G., Martin, C., Beuckelaers, W., Zdravkovic, L., Taborda, D., Potts, D., Jardine, R. *et al.* (2017). Pisa: New design methods for offshore wind turbine monopiles. In *Offshore Site Investigation Geotechnics 8th International Conference Proceeding*, vol. 142, Society for Underwater Technology, pp. 142–161.

Chong, S.-H. & Santamarina, J. C. (2016). Sands subjected to repetitive vertical loading under zero lateral strain: accumulation models, terminal densities, and settlement. *Canadian Geotechnical Journal* **53**, No. 12, 2039–2046.

Corciulo, S., Zanoli, O. & Pisanò, F. (2017). Transient response of offshore wind turbines on monopiles in sand: role of cyclic hydro–mechanical soil behaviour. *Computers and Geotechnics* **83**, 221–238.

Corti, R., Diambra, A., Muir Wood, D., Escribano, D. E. & Nash, D. F. (2016). Memory surface hardening model for granular soils under repeated loading conditions. *Journal of Engineering Mechanics* , 04016102.

Corti, R., Gourvenec, S. M., Randolph, M. F. & Diambra, A. (2017). Application of a memory surface model to predict whole-life settlements of a sliding foundation. *Computers and Geotechnics* **88**, 152–163.

Dafalias, Y. F. & Manzari, M. T. (2004). Simple plasticity sand model accounting for fabric change effects. *Journal of Engineering mechanics* **130**, No. 6, 622–634.

Dappolonia, D. & Dappolonia, E. (1967). Determination of the maximum density of cohesionless soils. In *Asian Conf Soil Mech & Fdn E Proc/Is/.*

DNV, G. (2016). Dnvgl-st-0126,. *Support structures for wind turbines* .

Galavi, V., Beuth, L., Coelho, B. Z., Tehrani, F. S., Hölscher, P. & Van Tol, F. (2017). Numerical simulation of pile installation in saturated sand using material point method. *Procedia Engineering* **175**, 72–79.

Houlsby, G., Abadie, C., Beuckelaers, W. & Byrne, B. (2017). A model for nonlinear hysteretic and ratcheting behaviour. *International Journal of Solids and Structures* **120**, 67–80.

Jostad, H., Grimstad, G., Andersen, K., Saue, M., Shin, Y. & You, D. (2014). A fe procedure for foundation design of offshore structures–applied to study a potential owt monopile foundation in the korean western sea. *Geotechnical Engineering Journal of the SEAGS & AGSSEA* **45**, No. 4, 63–72.

Kementzetzidis, E., Corciulo, S., Versteijlen, W. & Pisanò, F. (2018a). Geotechnical aspects of offshore wind turbine dynamics from 3d non-linear soil-structure simulations. *Soil Dynamics and Earthquake Engineering* **0**.

Kementzetzidis, E., Versteijlen, W. G., Nernheim, A. & Pisanò, F. (2018b). 3d FE dynamic modelling of offshore wind turbines in sand: natural frequency evolution in the pre–to after-storm transition. In *Proceedings of the 9th european conference on numerical methods in geotechnical engineering (NUMGE 2018), june 25-27, 2018, porto, Portugal*, CRC Press, pp. 1477–1484.

Lackenby, J., Indraratna, B., McDowell, G. & Christie, D. (2007). Effect of confining pressure on ballast degradation and deformation under cyclic triaxial loading. *Gotechnique* **57**, No. 6, 527–536, doi: 10.1680/geot.2007.57.6.527.

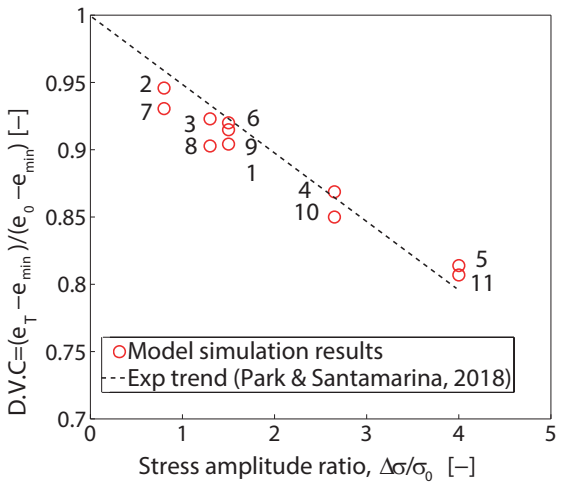

Fig. 5. Dimensionless volume contraction λ against cyclic stress amplitude ratio $\Delta\sigma/\sigma_0$. Numbering of simulation points refers to test numbers in Table 1.

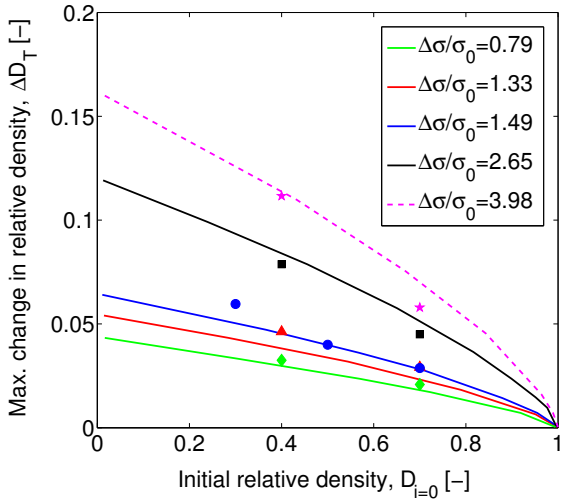

Fig. 6. Maximum changes in relative density ΔD_T against initial/pre-cyclic values $D_{i=0}$ – dash lines: interpolation of Park & Santamarina's data; markers: model simulations; same colours assigned to related dash lines and markers.

LeBlanc, C., Houlsby, G. & Byrne, B. (2010). Response of stiff piles in sand to long-term cyclic lateral loading. *Geotechnique* **60**, No. 2, 79–90.

Lekarp, F. & Dawson, A. (1998). Modelling permanent deformation behaviour of unbound granular materials. *Construction and building materials* **12**, No. 1, 9–18.

Lin, H., Suleiman, M. T., Brown, D. G. & Kavazanjian Jr, E. (2015). Mechanical behavior of sands treated by microbially induced carbonate precipitation. *Journal of Geotechnical and Geoenvironmental Engineering* **142**, No. 2, 04015066.

Liu, H., Abell, J. A., Diambra, A. & Pisan, F. (2018a). Modelling the cyclic ratcheting of sands through memory- enhanced bounding surface plasticity. *Gotechnique* **0**, No. 0, 1–57, doi:10.1680/jgeot.17.p.307.

Liu, H., Zygounas, F., Diambra, A. & Pisanò, F. (2018b). Enhanced plasticity modelling of high-cyclic ratcheting and pore pressure accumulation in sands. In *Numerical Methods in Geotechnical Engineering IX: Proceedings of the 9th European Conference on Numerical Methods in Geotechnical Engineering (NUMGE 2018), June 25-27, 2018, Porto, Portugal*, CRC Press, p. 87.

López-Querol, S. & Coop, M. (2012). Drained cyclic behaviour of loose dogs bay sand. *Géotechnique* **62**, No. 4, 281–289.

Narsilio, A. & Santamarina, J. (2008). Terminal densities. *Geotechnique* **58**, No. 8, 669.

Park, J. & Santamarina, J. (2018). Sand response to a large number of loading cycles under zero-lateral strain conditions: Evolution of void ratio and small strain stiffness. *Géotechnique* , 1–44.

Pasten, C., Shin, H. & Santamarina, J. C. (2013). Long-term foundation response to repetitive loading. *Journal of Geotechnical and Geoenvironmental Engineering* **140**, No. 4, 04013036.

Pisanò, F., Schipper, R. & Schreppers, G.-J. (2019). Input of fully 3d FE soil-structure modelling to the operational analysis of jack-up structures. *Marine Structures* **63**, 269–288.

Santamarina, J. C. & Cho, G. C. (2001). Determination of critical state parameters in sandy soilssimple procedure. *Geotechnical testing journal* **24**, No. 2, 185–192.

Taiebat, M. & Dafalias, Y. F. (2008). Sanisand: Simple anisotropic sand plasticity model. *International Journal for Numerical and Analytical Methods in Geomechanics* **32**, No. 8, 915–948.

Triantafyllidis, T., Wichtmann, T., Chrisopoulos, S., Zachert, H. *et al.* (2016). Prediction of long-term deformations of offshore wind power plant foundations using engineer-oriented models based on HCA. In *The 26th International Ocean and Polar Engineering Conference*, International Society of Offshore and Polar Engineers.

Wichtmann, T. (2005). *Explicit accumulation model for non-cohesive soils under cyclic loading*. Ph.D. thesis, Inst. für Grundbau und Bodenmechanik Bochum University, Germany.

Wichtmann, T. & Triantafyllidis, T. (2016). An experimental database for the development, calibration and verification of constitutive models for sand with focus to cyclic loading: part itests with monotonic loading and stress cycles. *Acta Geotechnica* **11**, No. 4, 739–761.

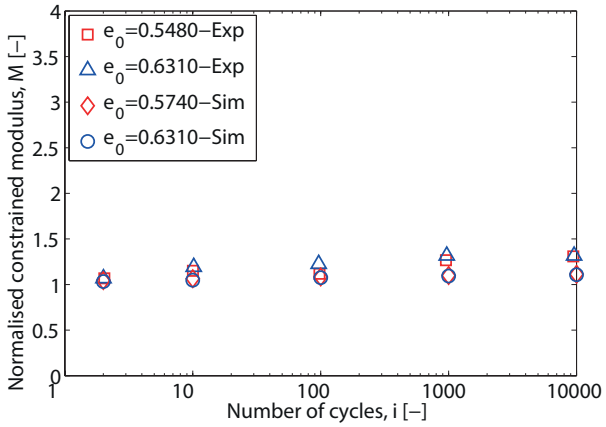

(a) $\Delta\sigma/\sigma_0 = 1.3$

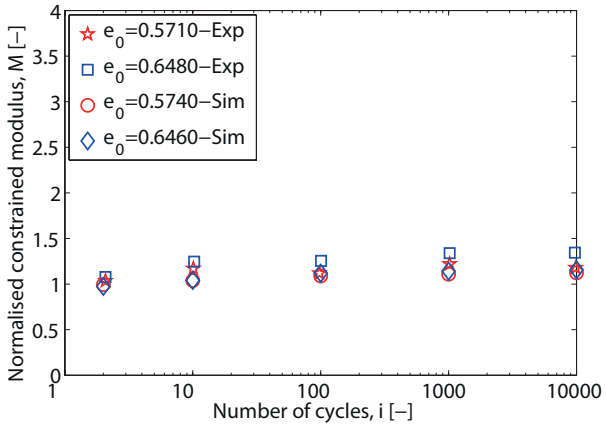

(b) $\Delta\sigma/\sigma_0 = 2.7$

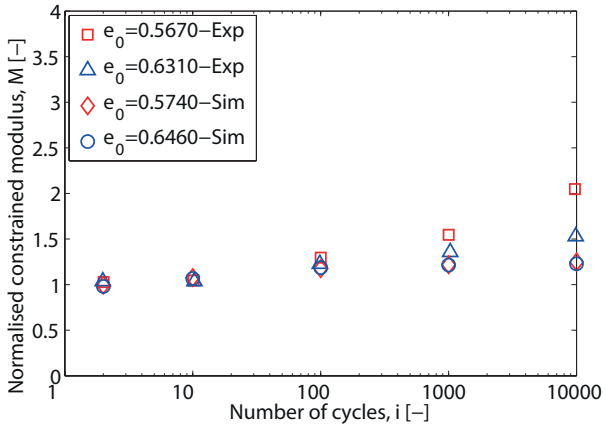

(c) $\Delta\sigma/\sigma_0 = 4.0$

Fig. 7. Evolution of constrained modulus M with increasing loading cycle N. Stress amplitude ratio: (a) $\Delta\sigma/\sigma_0 = 1.3$; (b) $\Delta\sigma/\sigma_0 = 2.7$; (c) $\Delta\sigma/\sigma_0 = 4.0$.